Korean J. Chem. Eng., 34(5), 1576-1583 (2017)
DOI: 10.1007/s11814-017-0044-y

pISSN: 0256-1115
eISSN: 1975-7220

NH_3-SCR performance and characterization over magnetic iron-magnesium mixed oxide catalysts

Liting Xu*, Shengli Niu*, Chunmei Lu*,†, Dong Wang, Kang Zhang*, and Jing Li*****

*School of Energy and Power Engineering, Shandong University, 250061 Jinan, China
**State Key Joint Laboratory of Environment Simulation and Pollution Control, Tsinghua University, Beijing 100084, China
***School of Chemistry and Chemical Engineering, Shandong University, 250100 Jinan, China
(*Received 14 July 2016 • accepted 17 February 2017*)

Abstract−A series of magnetic iron-magnesium mixed oxide catalysts ($Fe_{1-x}Mg_xO_z$) were synthesized via a novel co-precipitation method with microwave thermal treatment, and their activity in NH_3-SCR was tested on a quartz fixed-bed reactor. Physical and chemical properties of the catalysts were characterized by X-ray diffraction (XRD), N_2-adsorption-desorption, scanning electron microscopy (SEM) and energy dispersive spectrometry (EDS). $Fe_{0.8}Mg_{0.2}O_z$ with excellent N_2 selectivity and resistance to SO_2 and H_2O was validated as the proper SCR catalyst, with the maximum NO_x conversion of 99.1% fulfilled at 325 °C. Activity was strongly influenced by the γ-Fe_2O_3 crystalline phase, and magnesium existed in an amorphous phase and interacted with iron oxide intensively to form solid solution in favor of SCR. For $Fe_{0.8}Mg_{0.2}O_z$ catalyst, optimum pore diameter distribution, appropriate surface area, pore volume and abundant lattice oxygen on the surface could be guaranteed, which is good for the diffusion process and enhances the activity.

Keywords: Selective Catalytic Reduction (SCR), Catalyst, γ-Fe_2O_3, Magnesium, NO_x Conversion

INTRODUCTION

As one of the primary pollutants, nitrogen oxides (NO_x, mainly NO and NO_2) from coal-fired power plants and automobile exhaust have caused nitric acid rain, photochemical frog, ozone layer destruction, etc., which strongly affects human health and intensifies environmental pollution [1,2]. NO_x emission has become an international issue. Selective catalytic reduction (SCR) of NO_x with NH_3 is the most efficient method widely applied in coal-fired power plants to remove NO_x. As the core of SCR, catalysts determine the denitration efficiency and operating costs [3]. Manufacturing cost of the commercial V_2O_5-WO_3(MoO_3)/TiO_2 catalyst [4-6] widely used in industry is high, which is not good for mass production. In addition, the biological toxicity of V_2O_5 to the environment and human health will lead to secondary contamination, thus the Ministry of Environmental Protection stipulated that the commercial vanadium-titanium catalyst should be managed under tighter supervision and local regulation also claimed that V_2O_5 cannot be detected in SCR catalyst in China. Therefore, the development of environmentally friendly and efficient catalysts makes great sense. In such instances, iron-based catalysts [7] have become a hotspot in this field because of low cost, extensive sources, absence of toxicity, favorable SCR activity and N_2 selectivity. Cao [8] prepared Fe-Mn-Ce/γ-Al_2O_3 catalyst via sol-gel method and found that the addition of Fe sharply increased BET surface area and pore volume, and enhanced the acid sites on the surface of catalyst, which was in favor of SCR. The activity of Fe-Er-V/TiO_2-WO_3-SiO_2 catalyst [9] prepared via precipitation was directly related to the amount of Fe, and the interaction between Fe and Er could enhance the activity and stability of the catalyst. 80%-85% NO_x conversion could be achieved over 3 wt%Fe/WO_3-ZrO_2 catalyst [10] prepared by impregnation, because the Lewis acid sites formed on the surface of the catalyst with Fe addition. Research [11] showed that the maximum NO_x conversion of Fe_3O_4 catalyst just reached 15%, while γ-Fe_2O_3 catalyst could be up to 90% at 250 °C, and over 250 °C segmental formation of α-Fe_2O_3 led to the drop of SCR activity. The γ-Fe_2O_3 catalyst [12] prepared through co-precipitation method with microwave thermal treatment by Wang could reach 70% NO_x conversion at 300 °C, and the catalyst modified by Sn and Ti exhibited better SCR activity; among them, the activity of γ-$Fe_{0.95}Ti_{0.05}O_z$ catalyst approached 98%. Zhang [13] investigated the influence of calcination temperature of γ-Fe_2O_3 catalyst modified by Mn and concluded that 300 °C was the best calcination temperature and α-Fe_2O_3 formed at 400 °C and 450 °C badly affected SCR activity. The NO_x conversion of magnesium-based catalysts [14] prepared by co-mixed method for direct catalytic decomposition of nitrogen oxides in flue gas could be close to 85%-89%, while Mn-Mg-O_x catalyst [15] prepared via low-temperature solid phase method revealed excellent low temperature SCR activity and sulfur tolerance. However, there are few reports about γ-Fe_2O_3 catalysts modified by magnesium. In the current context, the magnetic iron-magnesium mixed oxide catalysts with different doping ratio of magnesium were prepared via a novel co-precipitation method with microwave thermal treatment, and their SCR activities were investigated in a quartz fixed-bed reactor. The physical and chemical properties of the catalysts, such as crystalline phase, BET surface area, pore diameter distribu-

†To whom correspondence should be addressed.
E-mail: cml@sdu.edu.cn
‡The paper will be reported in the 11th China-Korea Clean Energy Workshop.

tion and micro-morphology were characterized by X-ray diffraction (XRD), N_2-adsorption-desorption, scanning electron microscopy (SEM) and energy dispersive spectrometry (EDS), to reveal the effect of different doping ratio of magnesium on the magnetic iron-magnesium mixed oxide catalysts. Our aim is to build a foundation for the development of a novel, environmentally friendly, magnetic iron-magnesium mixed oxide catalyst.

EXPERIMENTAL

1. The Preparation of Catalysts

$FeSO_4{\cdot}7H_2O$, $Mg(NO_3)_2{\cdot}6H_2O$, $NH_3{\cdot}H_2O$ (25%) and Na_2CO_3 used in the experiment are analytically pure and provided by Tianjin Kermel Chemical Reagent Co., Ltd. Gases used were provided by Jinan Deyang Special Gas Co., Ltd.

A series of magnetic iron-magnesium mixed oxide catalysts were synthesized via a novel co-precipitation method with microwave thermal treatment and denoted as $Fe_{1-x}Mg_xO_z$, where x (0, 0.1, 0.2, 0.3, 0.4, 0.5) represented the molar fraction of Mg/(Mg+Fe) in catalyst, and z represented the oxygen mole number. First, a certain amount of $FeSO_4{\cdot}7H_2O$ and $Mg(NO_3)_2{\cdot}6H_2O$ was dissolved in distilled water to get a mixed solution. The solution was stirred for 1h until fully dissolved, and then slowly titrated into 2 mol/L ammonia solution until pH of the mixed solution became 9-10. The precipitate was filtered and washed with distilled water for several times to remove foreign ions, and then impregnated with 1 mol/L Na_2CO_3 solution before disposed by microwave thermal treatment to get precursor. The total time of microwave thermal treatment was 25 min. The microwave, with radiation power of 700 W, radiates for 8 s and then stops for 14 s to form a work cycle with 22 s. The precursor washed by distilled water was desiccated at 105 °C for 10 h, followed by calcination at 400 °C for 5 h in air. The samples were crushed and sieved into 40-60 mesh (0.28 mm-0.45 mm) for test.

2. Catalysts Characterization

The X-ray diffraction was performed on a Rigaku D/max 2500 PC diffractometer with Cu Ka radiation, 50 kV×150 mA. The data of the 2θ from 10° to 90° were collected at 4°/min with the step size 0.1°. N_2-adsorption-desorption over catalysts were obtained at −196 °C using ASAP2020 surface area and porosity analyzer provided by Micromeritics Instrument Corporation, American. Specific surface area and average pore diameter were analyzed by using Brunauer-Emmett-Teller (BET) equation, while specific pore volume and pore diameter distribution were obtained by Barrett-Joyner-Halenda (BJH) method. Micro-morphology was characterized by using cold field emission scanning electron microscope (SEM, JSM-6700F, Japan). Qualitative and quantitative analysis of surface elements of the catalysts were carried out by energy dispersive spectrometer (EDS, Be4-U92, Oxford INCA X sight, OIMS, UK).

3. Activity Measurement

The NH_3-SCR activity was performed in a quartz fixed-bed reactor at ambient pressure. The flue gas was simulated through blending different gaseous reactants controlled by mass flowmeters. The reaction conditions were as follows: catalyst used in each experiment was 4 ml and the total flow rate was 2 L/min including 0.1 vol% NO, 0.1 vol% NH_3, 3.5 vol% O_2 and balanced N_2, the corresponding gas hourly space velocity (GHSV) was 30,000/h^{-1}, which is large enough to ensure high SCR activity of the catalyst in complex conditions under industrial application. The concentrations of NO and NO_2 in the inlet and outlet were analyzed by MGA5 flue gas analyzer (York Instrument, MRU, Germany), and the concentration of N_2O and NH_3 was monitored by Finland FTIR flue gas analyzer GASMET DX400. Data were collected every 25 °C from 100 °C to 400 °C. NO_x conversion and N_2 selectivity was calculated as follows:

$$\eta = \frac{\varphi_{NO_x(inlet)} - \varphi_{NO_x(outlet)}}{\varphi_{NO_x(inlet)}} \times 100\% \quad (1)$$

$$s_{N_2} = \frac{\varphi_{NO_x(inlet)} + \varphi_{NH_3(inlet)} - 2\varphi_{N_2O(outlet)}}{\varphi_{NO_x(inlet)} + \varphi_{NH_3(inlet)}} \times 100\% \quad (2)$$

where $\varphi_{NO_x(inlet)}$ and $\varphi_{NO_x(outlet)}$ mean the concentration of NO_x in the inlet and outlet of the reactor, while $\varphi_{NH_3(inlet)}$ and $\varphi_{N_2O(outlet)}$ denote

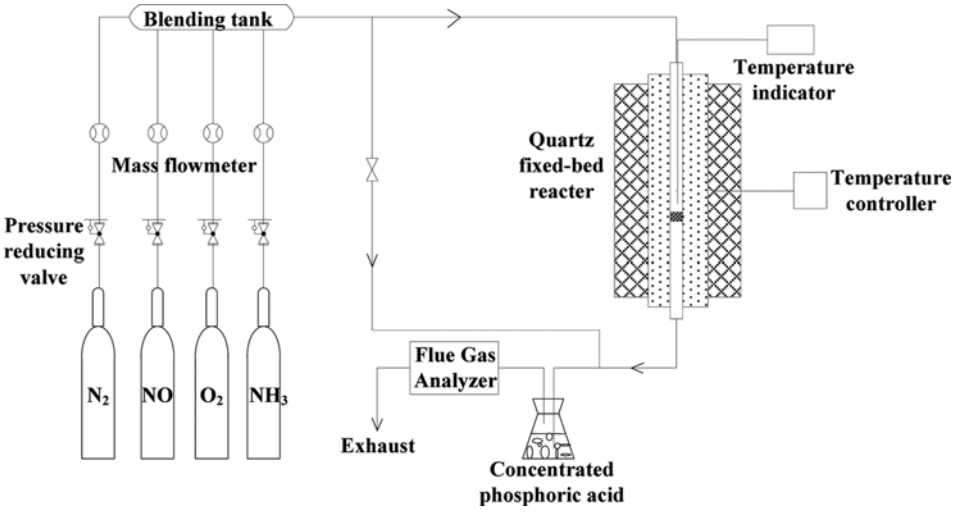

Fig. 1. Schematic diagram of NH_3-SCR test of flue gas with a quartz fixed-bed reactor.

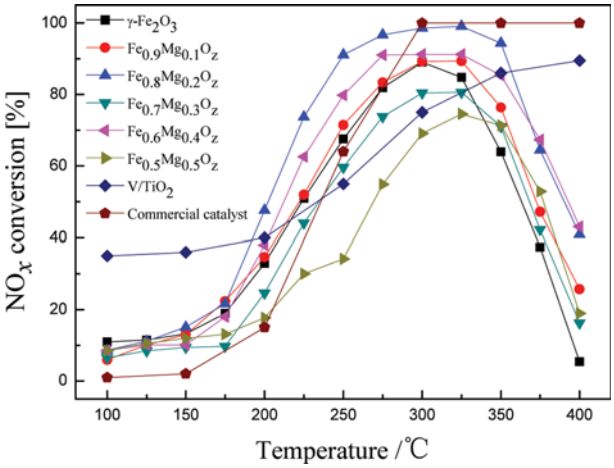

Fig. 2. NH_3-SCR activity over $Fe_{1-x}Mg_xO_z$ catalysts.

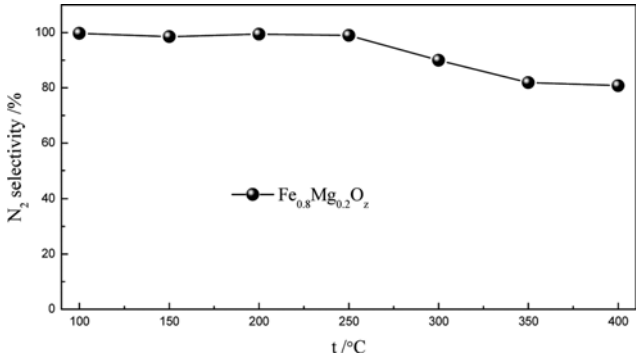

Fig. 3. N_2 selectivity in the NH_3-SCR reaction over $Fe_{0.8}Mg_{0.2}O_z$ catalyst.

the concentration of NH_3 and N_2O in the inlet and outlet, μL/L. NO_x represent the sum of NO and NO_2.

RESULTS

1. NH_3-SCR Activity

Fig. 2 shows the NH_3-SCR activity over $Fe_{1-x}Mg_xO_z$ catalysts and γ-Fe_2O_3 catalyst. From the results, NO_x conversions of all the catalysts gradually increase to the maximum as the temperature increases. The increase in temperature can exacerbate the thermal motion of molecules, so accelerate the reaction between NH_3 and NO. However, when the temperature keeps increasing, the NO_x conversions decrease due to the oxidation of NH_3.

Among all the catalysts, $Fe_{0.8}Mg_{0.2}O_z$ catalyst shows the best activity widely ranged with NO_x conversion above 90% from 250 to 350 °C, and the maximum NO_x conversion can reach 99.1% at 325 °C. Compared with $Fe_{0.8}Mg_{0.2}O_z$ catalyst, γ-Fe_2O_3 catalyst supplies a narrow temperature window with the maximum NO_x conversion of less than 90%. In general, from 100 to 400 °C, the NH_3-SCR activity decreases in the following sequence: $Fe_{0.8}Mg_{0.2}O_z$> $Fe_{0.6}Mg_{0.4}O_z$>$Fe_{0.9}Mg_{0.1}O_z$>γ-Fe_2O_3>$Fe_{0.7}Mg_{0.3}O_z$>$Fe_{0.5}Mg_{0.5}O_z$.

The experiment results indicate that the appropriate amount of magnesium doped in γ-Fe_2O_3 catalyst can not only improve activity, but also effectively broaden the temperature window of catalyst. However, when the doping ratio of magnesium is too large, compared with γ-Fe_2O_3 catalyst, the activity and temperature windows of the catalysts go down. The analysis supports that the main active component of the catalyst is γ-Fe_2O_3, while magnesium shows little activity in the catalyst as assistant [16] and affects the activity in two aspects. The addition of magnesium can optimize the microstructure of the catalyst to improve the activity, but the increase of magnesium will cause a decrease in the main active component γ-Fe_2O_3, weakening the denitration performance of the catalyst [17], and these two aspects codetermine the activity of catalyst.

The activities of $Fe_{1-x}Mg_xO_z$ catalysts were also compared with that of V/TiO_2 catalyst prepared in previous work and a commercial catalyst in Fig. 2. It can be concluded that the maximum NO_x conversion of V/TiO_2 catalyst was less than 90%, and the temperature window of the commercial catalyst ranged from 300 to 400 °C with NO_x conversion approaching 100%. The NO_x conversion of $Fe_{1-x}Mg_xO_z$ catalysts increased rapidly from 200 to 250 °C than V/TiO_2 catalyst. Especially, the NO_x conversion of $Fe_{0.8}Mg_{0.2}O_z$ catalyst increased fast from 47.6% at 200 °C to 99.1% at 250 °C. The temperature window of $Fe_{0.8}Mg_{0.2}O_z$ catalyst was 50 °C lower than that of the commercial catalyst, and the NO_x conversion of it below 300 °C was much higher than the commercial catalyst. In consideration of the high cost of the commercial catalyst and the biological toxicity of V_2O_5 to environment and human health, it is necessary to do further research on environmentally friendly $Fe_{0.8}Mg_{0.2}O_z$ catalyst with high SCR activity, wide and low temperature window, low cost, etc.

2. N_2 Selectivity and Effects of SO_2 and H_2O over $Fe_{0.8}Mg_{0.2}O_z$ Catalyst

Since NH_3 can selectively react with NO to form N_2 and H_2O, rather than being oxidized by O_2, the reaction is said to be "selective". To avoid the deviation caused by N_2O, Fig. 3 shows the N_2 selectivity in the NH_3-SCR reaction over $Fe_{0.8}Mg_{0.2}O_z$ catalyst. The N_2 selectivity over $Fe_{0.8}Mg_{0.2}O_z$ catalyst approaches 100% below 250 °C, which means nearly no N_2O is released. From 300 to 400 °C, the N_2 selectivity slowly decreases to 80.8%, indicating that the emission of N_2O is less than 0.002 vol%.

To further reveal the catalytic activity, the resistance of SO_2 and H_2O were investigated over $Fe_{0.8}Mg_{0.2}O_z$ catalyst, as shown in Fig. 4. NO_x conversion about 94% was obtained after steady operation for 1 h at 350 °C. In the case of 8 vol% water vapor, an obvious decrease in NO_x conversion from 94% to 84% occurred in 1 h due to the competitive adsorption of H_2O and NH_3 on the surface of the catalyst. Then the NO_x conversion could maintain around 88% in 12 h. Stopping adding H_2O, desorption of H_2O from the surface made NO_x conversion gradually come back to 95%, which proves that the deactivation of $Fe_{0.8}Mg_{0.2}O_z$ catalyst with H_2O is reversible. In the presence of 0.03 vol% SO_2, the NO_x conversion dropped to 84% in 1 h, and then slightly decreased to about 75% in 10 h. The deposition of NH_4HSO_4 and $(NH_4)_2SO_4$ on the surface of $Fe_{0.8}Mg_{0.2}O_z$ catalyst was the main reason that made the NO_x conversion decrease. As the deposition and decomposition of NH_4HSO_4 and $(NH_4)_2SO_4$ came to a steady state, the NO_x conversion fluctuated in a small range from 70% to 75% within 100 h. The results demonstrate

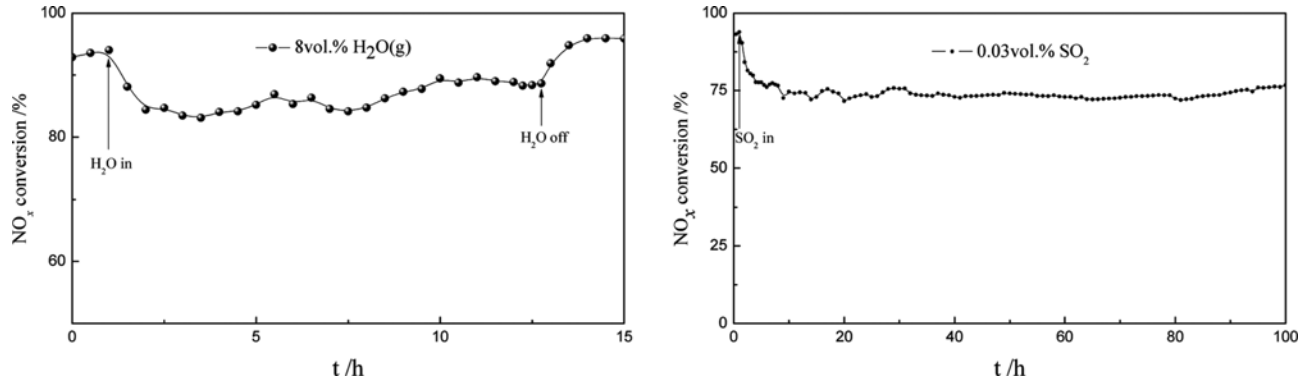

Fig. 4. Effect of H_2O and SO_2 on NO_x conversion over $Fe_{0.8}Mg_{0.2}O_z$ catalyst.

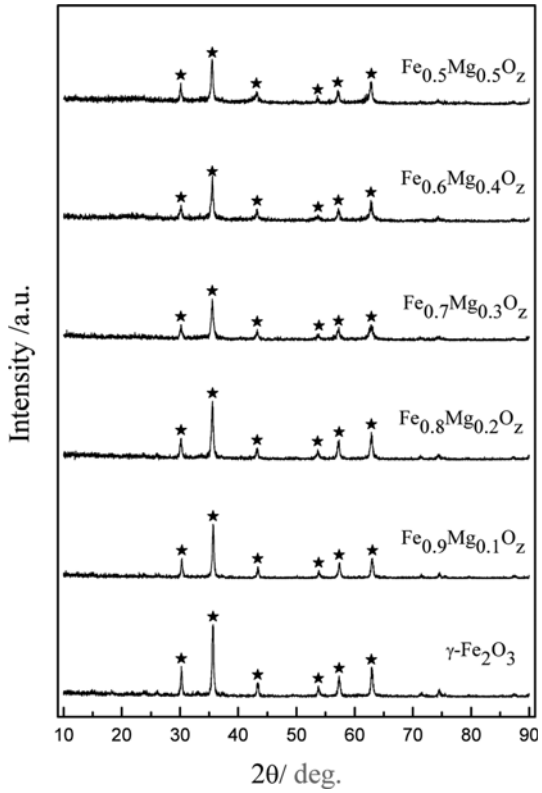

Fig. 5. Powder XRD patterns of $Fe_{1-x}Mg_xO_z$ catalysts.

that good resistance to H_2O and SO_2 was gained over $Fe_{0.8}Mg_{0.2}O_z$ catalyst.

3. XRD

Powder XRD patterns of $Fe_{1-x}Mg_xO_z$ catalysts are shown in Fig. 5. Similar to γ-Fe_2O_3 catalyst, obvious sharp diffraction peaks of γ-Fe_2O_3 crystallite over $Fe_{1-x}Mg_xO_z$ catalysts are observed at 2θ= 30.18°, 35.58°, 43.28°, 53.66°, 57.32° and 62.86°, according to #39-1346 in Joint Committee on Powder Diffraction Standards (JCPDS) [18], and the intensity of the peaks due to γ-Fe_2O_3 crystallite decreases with increasing Mg content. Analysis based on Debye-Scherrer equation indicates that the addition of magnesium can decrease the crystallinity and the diameter of γ-Fe_2O_3 crystallite, which refines the γ-Fe_2O_3 crystallite. In addition, there are no magnesium oxide diffraction peaks observed, implying that γ-Fe_2O_3 crystallite is the real active phase, which is in accordance with the surmise above. Magnesium oxides that existed as an amorphous phase in catalyst and highly disperse on the surface of the catalyst can interact with iron oxide intensively to form solid solution, which is in favor of SCR activity.

Table 1. Textural properties of $Fe_{1-x}Mg_xO_z$ catalysts

Samples	S_{BET}/ $m^2 \cdot g^{-1}$	Pore volume/ $cm^3 \cdot g^{-1}$	Average pore diameter/ nm
γ-Fe_2O_3	27.93	0.15	21.21
$Fe_{0.9}Mg_{0.1}O_z$	30.62	0.15	19.31
$Fe_{0.8}Mg_{0.2}O_z$	44.00	0.19	16.83
$Fe_{0.7}Mg_{0.3}O_z$	60.12	0.25	16.33
$Fe_{0.6}Mg_{0.4}O_z$	88.94	0.31	13.60
$Fe_{0.5}Mg_{0.5}O_z$	102.64	0.32	12.71

4. N_2-adsorption-desorption

To better demonstrate the effect of magnesium on SCR activity over γ-Fe_2O_3, the microstructures of $Fe_{1-x}Mg_xO_z$ catalysts such as BET surface area, pore volume and pore diameter were tested through N_2-adsorption-desorption and given in Table 1. Magnesium sharply increases the surface area and the pore volume of γ-Fe_2O_3, which decreases the average pore diameter. The surface area and the pore volume gradually increase with the molar ratio of Mg/(Mg+Fe) increasing from 0 to 0.5. From XRD results, it is also concluded that the crystallinity and the diameter of γ-Fe_2O_3 crystallite can be refined with the addition of magnesium. Large surface area and pore volume can provide more active sites, and relatively small pore diameter [19,20] can promote the possibility of collision between reactant molecules and active sites, accordingly speed up the reaction. The results from activity tests of $Fe_{1-x}Mg_xO_z$ catalysts show that the activities are not always increased with the ratio of Mg/(Fe+Mg) increase. It is considered that γ-Fe_2O_3 is the real active component, as the amount of magnesium increases, γ-Fe_2O_3 crystalline dispersity and pore structures are improved, but the real active content of γ-Fe_2O_3 decreases. It is surmised that the ratio of Mg/(Fe+Mg) being 0.2 can guarantee the amount of the active component as well as the appropriate microstructures.

Micropores are calculated by t-Plot method, shown in Table 2. The ratio of external surface area and microporous area over $Fe_{1-x}Mg_xO_z$

Table 2. t-Plot properties of $Fe_{1-x}Mg_xO_z$ catalysts

Samples	t-Plot microporous area/$m^2 \cdot g^{-1}$	t-Plot external surface area/$m^2 \cdot g^{-1}$	t-Plot microporous volume/$cm^3 \cdot g^{-1}$
γ-Fe_2O_3	2.84	25.09	13.26×10^{-4}
$Fe_{0.9}Mg_{0.1}O_z$	3.04	27.59	14.17×10^{-4}
$Fe_{0.8}Mg_{0.2}O_z$	2.64	43.36	10.37×10^{-4}
$Fe_{0.7}Mg_{0.3}O_z$	3.57	56.55	14.59×10^{-4}
$Fe_{0.6}Mg_{0.4}O_z$	5.10	83.84	21.06×10^{-4}
$Fe_{0.5}Mg_{0.5}O_z$	5.36	97.27	21.2×10^{-4}

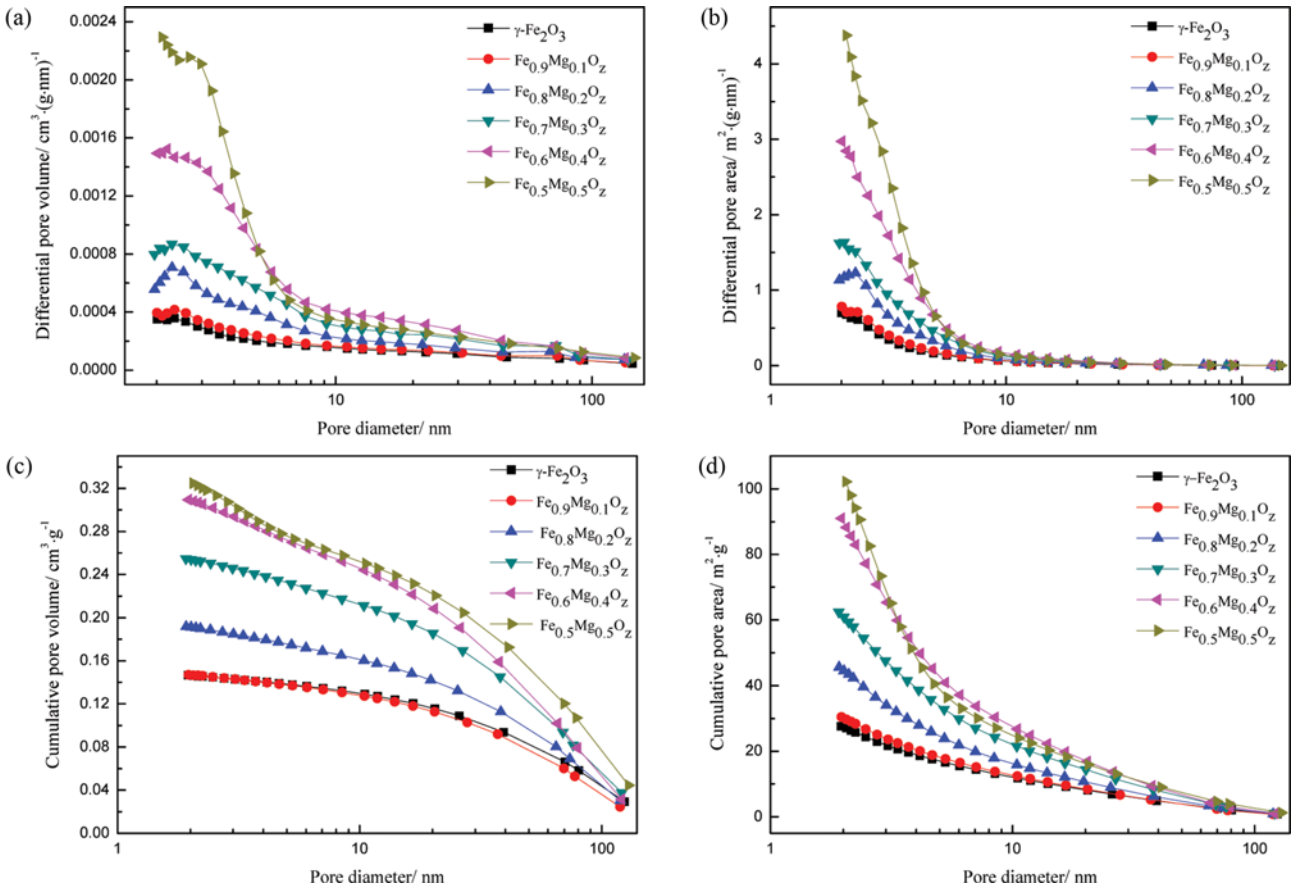

Fig. 6. Distribution characterization of pore structures over $Fe_{1-x}Mg_xO_z$ catalysts (a) Pore volume (b) Pore area (c) Cumulative pore volume (d) Cumulative pore area.

catalysts (where x increased from 0 to 0.5) are 8.83, 9.07, 16.42, 15.84, 16.44 and 18.15, and their micropores volumes are close to zero, indicating that there are substantially few micropores in $Fe_{1-x}Mg_xO_z$ catalysts.

Distribution characterization of pore structures over $Fe_{1-x}Mg_xO_z$ catalysts is shown in Fig. 6. Pore diameters of $Fe_{1-x}Mg_xO_z$ catalysts mainly distribute from 2 nm to 10 nm. Mesopores (2-50 nm) are major pore type and hardly any micropores are observed in $Fe_{1-x}Mg_xO_z$ catalysts.

For γ-Fe_2O_3 catalyst and $Fe_{0.9}Mg_{0.1}O_z$ catalyst, the amount of mesopores is fewer, which provides less surface area and pore volume. Mesopores range from 2 nm to 10 nm over $Fe_{0.6}Mg_{0.4}O_z$ catalyst and $Fe_{0.5}Mg_{0.5}O_z$ catalyst are abundant, but the sharp decrease of pores from 10 nm to 100 nm leads to the lack of macropores and causes the resistance of gaseous reactant diffusion increase. The ratio of mesopores and macropores over $Fe_{0.8}Mg_{0.2}O_z$ is suitable and distribution of pore diameter is reasonable, which can provide large surface area and pore volume, as well as guarantee the mass transfer and diffusion process.

N_2-adsorption-desorption isotherms of $Fe_{1-x}Mg_xO_z$ catalysts are shown in Fig. 7. According to IUPAC (International Union of Pure and Applied Chemistry) classification, N_2-adsorption-desorption isotherms of $Fe_{1-x}Mg_xO_z$ catalysts belong to V-shaped curve with H3 hysteresis loop. Gas-solid interaction in mesopores on the solid surface made isothermals present a V-shaped carve. The adsorbed volume is small when the relative pressure is low, but when the relative pressure approaches the saturated vapor pressure of nitrogen, capillary condensation initiates and the adsorbed volume sharply

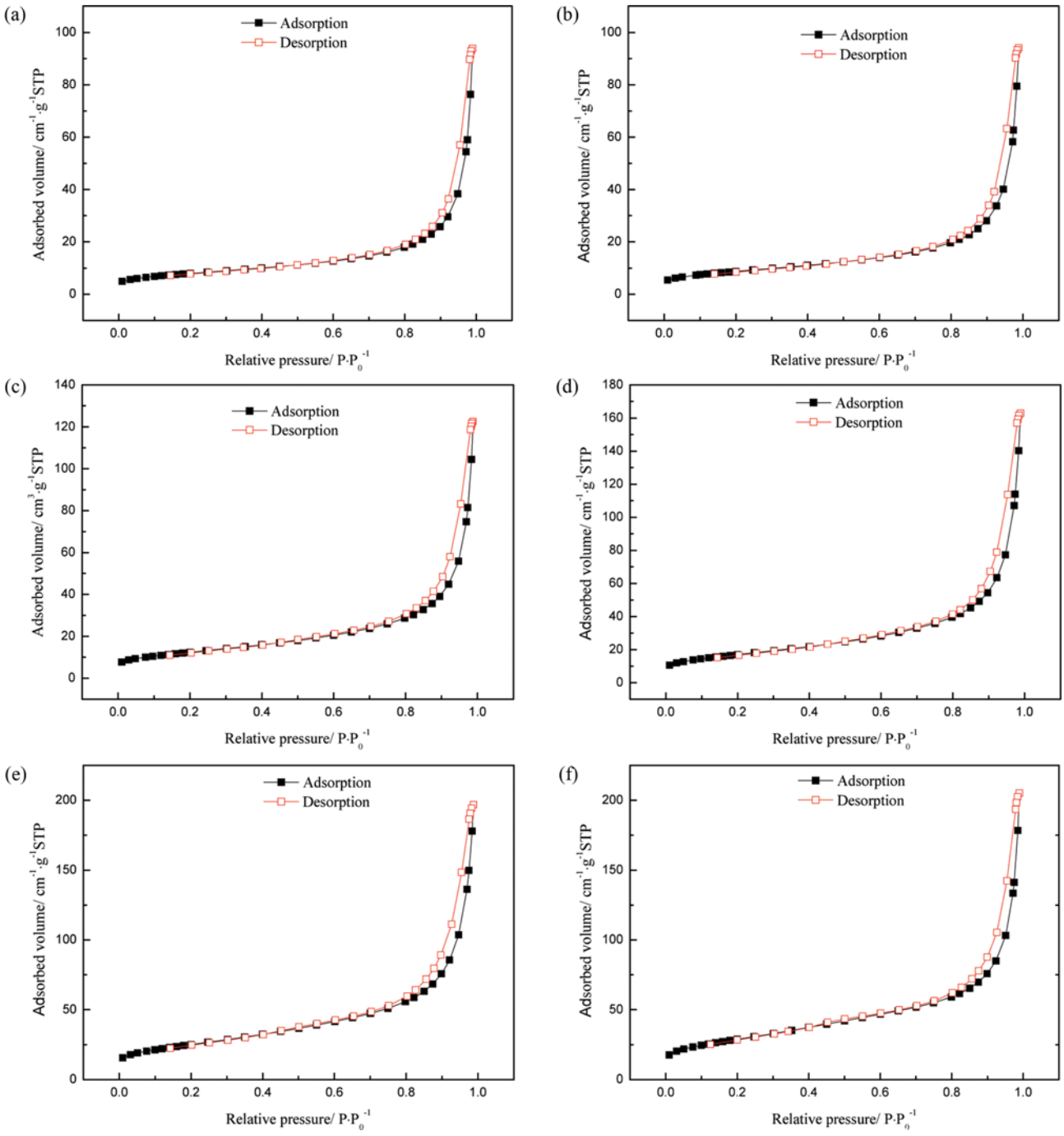

Fig. 7. N_2-adsorption-desorption isotherms of $Fe_{1-x}Mg_xO_z$ catalysts (a) γ-Fe_2O_3; (b) $Fe_{0.9}Mg_{0.1}O_z$; (c) $Fe_{0.8}Mg_{0.2}O_z$; (d) $Fe_{0.7}Mg_{0.3}O_z$; (e) $Fe_{0.6}Mg_{0.4}O_z$; (f) $Fe_{0.5}Mg_{0.5}O_z$.

increases. From H3 hysteresis loop, it can be inferred that there are wedge-shaped pores (slit pores) formed by particles packed loosely on the surface of the catalysts. The results indicate that there is a certain amount of mesopores (2-50 nm) and macropores (>50 nm) in the catalysts.

5. SEM and EDS

SEM images of $Fe_{1-x}Mg_xO_z$ catalysts are shown in Fig. 8. With the increase of the addition of magnesium in the catalysts, the regulation of particles distribution on the surface represents from sphere to acerose and laminar distribution. Small spherical particles pack closely in γ-Fe_2O_3 catalyst, and adhere to each other obviously, appear as reunion and accumulation phenomena. It will cause poor connectivity between pores and have a bad effect on SCR reaction.

Compared with γ-Fe_2O_3 catalyst, spherical particles of $Fe_{0.9}Mg_{0.1}O_z$ catalyst are relatively regular and there are no obvious reunion and accumulation phenomenon. Spherical particles of $Fe_{0.8}Mg_{0.2}O_z$ catalyst are the most regular and relatively independent of each other. The diameter of spherical particles in $Fe_{0.8}Mg_{0.2}O_z$ catalyst is iden-

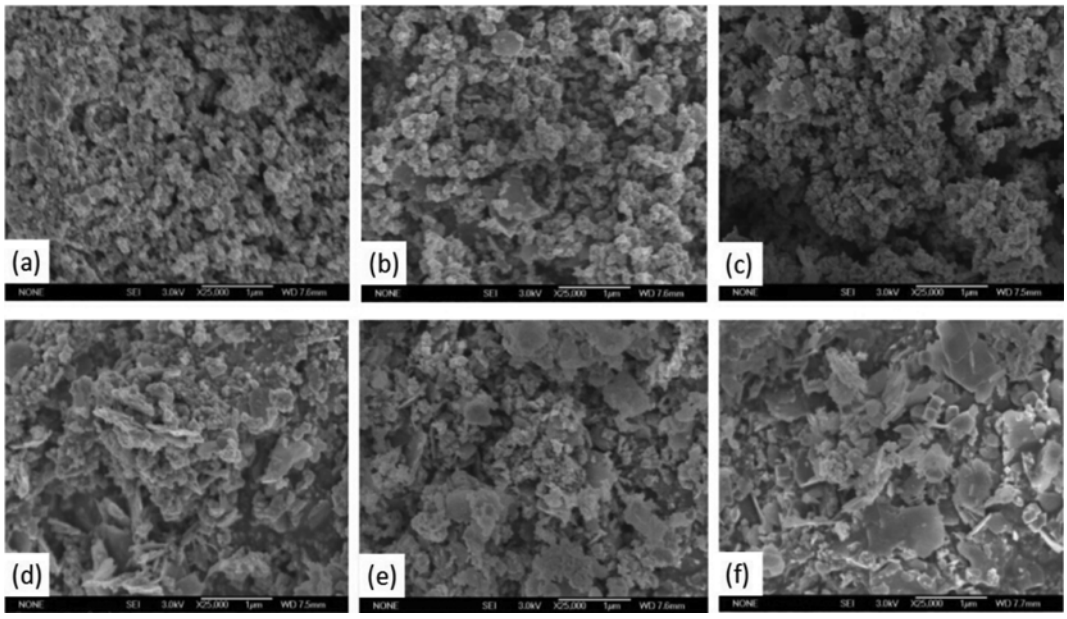

Fig. 8. SEM images of $Fe_{1-x}Mg_xO_z$ catalysts (a) γ-Fe_2O_3; (b) $Fe_{0.9}Mg_{0.1}O_z$; (c) $Fe_{0.8}Mg_{0.2}O_z$; (d) $Fe_{0.7}Mg_{0.3}O_z$; (e) $Fe_{0.6}Mg_{0.4}O_z$; (f) $Fe_{0.5}Mg_{0.5}O_z$.

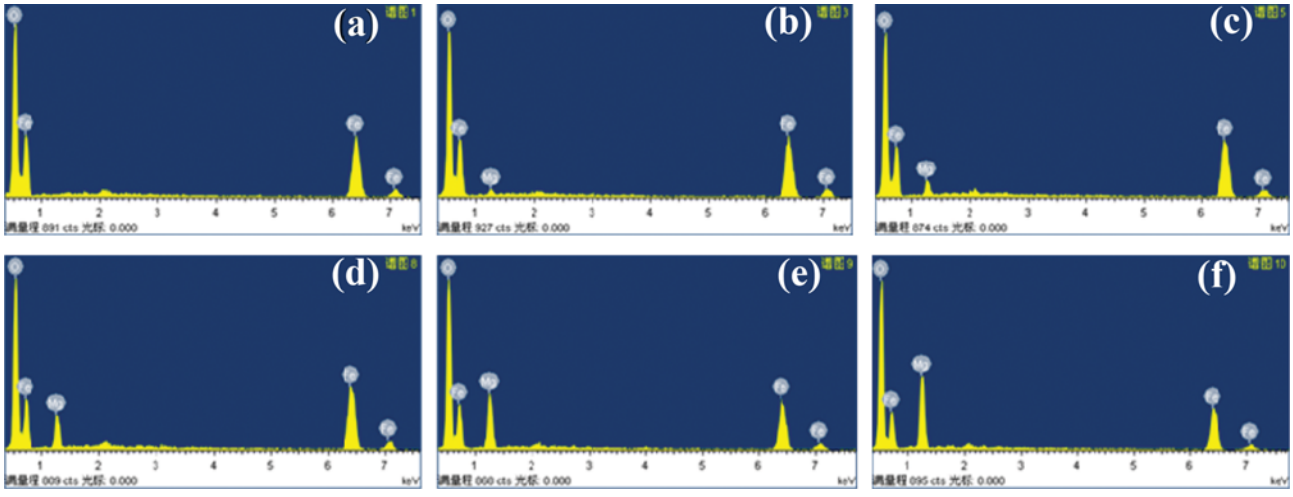

Fig. 9. EDS spectra of $Fe_{1-x}Mg_xO_z$ catalysts (a) γ-Fe_2O_3; (b) $Fe_{0.9}Mg_{0.1}O_z$; (c) $Fe_{0.8}Mg_{0.2}O_z$; (d) $Fe_{0.7}Mg_{0.3}O_z$; (e) $Fe_{0.6}Mg_{0.4}O_z$; (f) $Fe_{0.5}Mg_{0.5}O_z$.

tical, and the excellent connectivity between pores provides rich pore apertures for reactant gas to absorb and activate on the surface of catalyst in NH_3-SCR reaction, which are both in favor of mass transfer and diffusion process. Obvious particle accumulation phenomenon is observed on the surface of $Fe_{0.7}Mg_{0.3}O_z$ catalyst and presents acerose distribution while $Fe_{0.6}Mg_{0.4}O_z$ catalyst begins to show laminar distribution and pore apertures collapse. Meanwhile, there are hardly any pore structures observed in $Fe_{0.5}Mg_{0.5}O_z$ catalyst because of a large-scale patchy distribution and serious collapse of pore apertures. The diffusion of gaseous reactants and products in pore structures of catalyst has a great effect on denitration performance. Comprehensive analysis of the results of SEM and activity tests indicates that regular independent spherical distribution of particles can form the optimal pore structures and reduce the diffusion resistance of gaseous reactants in the catalyst, thus ensuring the mass transfer and diffusion process [21]. Additionally, more adsorption sites can be provided by large specific surface area and relatively small average pore diameter of spherical particles, which is beneficial for reaction and consistent with N_2-adsorption-desorption results.

EDS composition analysis of micro area on surface over $Fe_{1-x}Mg_xO_z$ catalysts is shown in Fig. 9. The main elements of $Fe_{1-x}Mg_xO_z$ catalysts are iron, magnesium and oxygen, which agrees with the expected active compositions.

Further analysis and disposition of EDS data over $Fe_{1-x}Mg_xO_z$ catalysts are done to obtain the percentage by weight and percentage by atomicity of surface elements, weight ratio and atomicity ratio of O/(Fe+Mg) on surface, and the results are shown in Table 3. The atomicity ratios of O/(Fe+Mg) over $Fe_{1-x}Mg_xO_z$ catalysts (where x increases from 0 to 0.5) are 1.63, 1.62, 1.68, 1.63, 1.50 and 1.44.

Table 3. EDS analysis data of $Fe_{1-x}Mg_xO_z$ catalysts

Catalyst	Percentage by weight/wt%			Percentage by atomicity/at%			O/(Fe+Mg)	
	Fe	Mg	O	Fe	Mg	O	Weight ratio	Atomicity ratio
γ-Fe_2O_3	68.19	-	31.81	38.05	-	61.95	0.47	1.63
$Fe_{0.9}Mg_{0.1}O_z$	66.40	1.31	32.29	36.46	1.65	61.89	0.48	1.62
$Fe_{0.8}Mg_{0.2}O_z$	63.87	2.56	33.57	34.17	3.15	62.69	0.51	1.68
$Fe_{0.7}Mg_{0.3}O_z$	58.83	6.56	34.61	30.21	7.74	62.04	0.53	1.63
$Fe_{0.6}Mg_{0.4}O_z$	54.05	11.41	34.54	26.91	13.05	60.03	0.53	1.50
$Fe_{0.5}Mg_{0.5}O_z$	35.49	16.46	35.49	22.91	18.03	59.06	0.69	1.44

Among them, the atomicity ratio of O/(Fe+Mg) over $Fe_{0.8}Mg_{0.2}O_z$ catalyst is the highest, exceeding 1.50 of Fe_2O_3 under normal circumstances. It is concluded that the appropriate addition of magnesium contributes to the enrichment of lattice oxygen on the surface of γ-Fe_2O_3 catalyst, and the surface oxidability of catalyst can be enhanced with the abundant amount of lattice oxygen and absorbed oxygen, which is the important condition to ensure high activity of catalyst and favorable to SCR reaction [22].

CONCLUSIONS

$Fe_{1-x}Mg_xO_z$ catalysts synthesized by a novel co-precipitation method with microwave thermal treatment were tested for their activities. From 100 to 400 °C, the NH_3-SCR activity decreased in the following sequence: $Fe_{0.8}Mg_{0.2}O_z$>$Fe_{0.6}Mg_{0.4}O_z$>$Fe_{0.9}Mg_{0.1}O_z$>γ-Fe_2O_3>$Fe_{0.7}Mg_{0.3}O_z$>$Fe_{0.5}Mg_{0.5}O_z$. $Fe_{0.8}Mg_{0.2}O_z$ catalyst showed the best activity and excellent N_2 selectivity in a wide temperature range with NO_x conversion above 90% from 250 to 350 °C; especially at 325 °C, the maximum NO_x conversion of 99.1% could be achieved. In the presence of 0.03 vol% SO_2 and 8 vol% H_2O, NO_x conversion over $Fe_{0.8}Mg_{0.2}O_z$ catalyst slightly decreased. Magnesium existed in an amorphous phase and interacted with iron oxide intensively to form solid solution. The suitable ratio of mesopores and macropores and reasonable pore diameter distribution of $Fe_{0.8}Mg_{0.2}O_z$ catalyst could provide large surface area and pore volume, as well as guarantee the mass transfer and diffusion process. Regular independent spherical distribution of particles could form the optimal pore structures of $Fe_{0.8}Mg_{0.2}O_z$ catalyst and provide more adsorption sites, which is beneficial to SCR reaction. The abundant amount of lattice oxygen and absorbed oxygen could enhance the surface oxidability of $Fe_{0.8}Mg_{0.2}O_z$ catalyst, which is in favor of SCR reaction.

ACKNOWLEDGEMENTS

This work was financially supported by the National Natural Science Foundation of China (51276101, 51576117) and the Fundamental Research Funds of Shandong University (2015JC024).

REFERENCES

1. J. Yang, H. T. Ma, Y. Yamamoto, J. Yu, G. W. Xu, Z. G. Zhang and Y. Suzuki, *Chem. Eng. J.*, **230**, 513 (2013).
2. Y. B. Jo, J. S. Cha, J. H. Ko, M. C. Shin, S. H. Park, J. K. Jeon, S. S. Kim and Y. K. Park, *KJCE*, **28**, 106 (2011).
3. Y. G. Chen, Z. Wang and Z. C. Guo, *Chin J. Process Eng.*, **7**, 632 (2007).
4. P. W. Seo, S. S. Kim and S. C. Hong, *KJCE*, **27**, 1220 (2010).
5. F. Y. Gao, X. L. Tang, H. H. Yi, S. Z. Zhao, T. T. Zhang, D. Li and D. Ma, *Bull. Sci. Technol.*, **26**, 2560 (2014).
6. L. Y. Xiong, Q. Zhong, Q. Q. Chen and S. L. Zhang, *KJCH*, **30**, 836 (2013).
7. X. Gao, X. J. Lu and M. H. Hu, *J. Jianghan Univ.*, **02**, 12 (2014).
8. F. Cao, S. Su, J. Xiang, P. Y. Wang, S. Hu, L. S. Sun and A. C. Zhang, *Fuel*, **139**, 232 (2015).
9. M. Casanova, J. Llorca, A. Sagar, K. Schermanz and A. Trovarelli, *Catal. Today*, **241**, 159 (2015).
10. R. Foo, T. Vazhnova, D. B. Luckyanov, P. Millington, J. collier, R. Rajaram and S. Golunski, *Appl. Catal. B-Environ.*, **162**, 174 (2015).
11. G. H. Yao, K. T. Gui and F. Wang, *Chem. Eng. Technol.*, **33**, 1093 (2010).
12. D. Wang, J. K. Wu, S. L. Niu, C. M. Lu, L. T. Xu, H. W. Yu and J. Li, *J. Fuel Chem. Technol.*, **43**, 876 (2015).
13. X. L. Zhang, D. Wang, J. S. Peng, C. M. Lu and L. T. Xu, *J. Fuel Chem. Technol.*, **43**, 243 (2015).
14. Y. Gao, X. M. Hu, P. J. Liu, Y. Li, Y. Zhang, Y. Liu and Y. B. Guo, *Chin J. Environ. Eng.*, **2**, 806 (2008).
15. R. Y. Lai, X. L. Tang, H. H. Yi, K. Li, P. Wang and X. Sun, *Mod. Chem. Ind.*, **34**, 76 (2014).
16. S. L. Zhang, H. Y. Li and Q. Zhong, *Appl. Catal. A-Gen.*, **435-436**, 156 (2012).
17. Z. Cao, Y. Huang, L. L. Peng and J. G Li, *J. Fuel Chem. Technol.*, **40**, 456 (2012).
18. J. S. Chen, X. S. Shang, J. P. Zhao, F. W. Zhang, Y. Xu and J. R. Li, *Electric. Power.*, **43**, 64 (2010).
19. S. Wang, G. H. Yao and K. T. Gui, *Prog. Chin. Soc. Electrial Eng.*, **29**, 47 (2009).
20. L. Chen, J. H. Li and M. F. Ge, *Environ. Sci. Technol.*, **44**, 9590 (2011).
21. L. Chen, J. H. Li, M. F. Ge and R. H. Zhu, *Catal. Today*, **153**, 77 (2010).
22. G. S. Qi and R. T. Yang, *J. Catal.*, **217**, 434 (2003).